International Journal of ChemTech Research
CODEN (USA): IJCRGG ISSN: 0974-4290
Vol.7, No.7, pp 3148-3154, 2015

ICEWEST-2015 [05th - 06th Feb 2015]
International Conference on Energy, Water and Environmental Science & Technology
PG and Research Department of Chemistry, Presidency College (Autonomous), Chennai-600 005, India

Synthesis and Characterization of Pd–Ir–Ni/C Electrocatalysts for Ethanol Oxidation in Membraneless Fuel Cells

S. Kiruthika and M. P. Rajesh*

Department of Chemical Engineering, SRM University, Chennai – 603 203,

Abstract: This paper presents the study on the investigation of high surface area carbon-supported Pd_{100}, $Pd_{40}Ni_{60}$, $Pd_{40}Ir_{60}$ and $Pd_{35}Ir_5Ni_{60}$ electrocatalysts in a membraneless fuel cell for the ethanol oxidation reduction at room temperature. The carbon-supported electrocatalysts were synthesized by simultaneous reduction method. The electrocatalysts were characterized in terms of structure, morphology and composition by using XRD and TEM techniques. X-ray diffractometry results confirmed the formation of Pd–Ir/C, Pd–Ni/C, Pd–Ir–Ni/C metal catalyst having typical Pd crystalline structure and the formation of Pd–Ir alloy. Transmission electron microscopy measurements revealed a decrease in the mean particle size of the catalysts for the ternary compositions. The structural change is beneficial for the catalytic activity of the compositions. The single membraneless ethanol fuel cell performances of the $Pd_{35}Ir_5Ni_{60}$/C, $Pd_{40}Ir_{60}$/C and $Pd_{40}Ni_{60}$/C anode catalysts were evaluated at room temperature. Among the catalysts investigated, the power density obtained for $Pd_{35}Ir_5Ni_{60}$/C (34 mW/cm^2) catalyst was higher than that of $Pd_{40}Sn_{60}$/C and $Pd_{40}Ni_{60}$/C , using 1.0 M ethanol + 1.0 M KOH as anode feed and 0.1 M sodium perborate + 1 M KOH as cathode feed.
Keywords: Iridium, Membraneless fuel cell, Palladium, Ternary Catalysts.

Introduction

With an increasing world population and advances in civilization, the energy consumption in the 20th century was marked with an unprecedented high. This trend of increasing energy consumption is likely to continue in the 21st century. Coupled with rapidly diminishing conventional energy sources, predominately based on fossil fuels, this increasing demand on energy has prompted various efforts around the world to explore alternative methods in harvesting energy[1, 5]. In particular, clean alternative energy sources are strongly preferred due to heightened awareness on the protection of the environment. Electrochemical power generation is one of the alternative energy-harvesting technologies that are attracting considerable interest due to its sustainability and environmental friendliness. Fuel cells are attractive devices to easily convert chemical energy into electricity[6, 7].

A prodigious amount of research has been conducted on the miniaturization of the conventional fuel cells. Although the energy density of the miniaturized fuel cells increases as their size continues to shrink, several technological and mechanical challenges including efficiency issues related to water and heat management, the ohmic over potential caused by the membrane, and fabrication difficulties still remain. Because of these limitations, novel designs are required to make a miniaturized fuel cell commercially viable[8, 9]. The microfluidic fuel cell is an innovative design with a great potential to overcome the current drawbacks of the miniaturized fuel cells, and become an inexpensive and reliable compact power source for practical applications.

Ethanol is a renewable and attractive fuel as it can be produced in great quantities from biomass and it is less toxic than methanol. However, its complete oxidation to CO_2 is more difficult than that of methanol due to the difficulty in C–C bond breaking and to the formation of CO-intermediates that poison the platinum anode catalysts. In this context, more active electrocatalysts are essential to enhance the ethanol electro-oxidation[10, 11].

The use of palladium as the anode catalyst for the ethanol oxidation reaction (EOR) in membraneless ethanol fuel cells (MLEFC) offers two significant advantages as compared with the use of Pt. First Pd shows both a higher catalytic activity and better stability for the EOR in alkaline media than Pt does. Secondly, Pd is more abundant than Pt and has a lower price, and thus the cost of fuel cell can be greatly reduced[12, 13]. Liang et al. studied the mechanism of the EOR on Pd in alkaline media by CV, and demonstrated that acetaldehyde was an active intermediate and acetate was the major product; the rate-determining step was the removal of adsorbed ethoxy intermediates by the OH_{ads} groups on Pd. In this regard, the effect of adding another component to Pd on the EOR has been intensively studied1[4, 16].

In the present work, we study the catalytic activity for the ethanol electro-oxidation reaction by incorporating a third metal Ni to the Pd–Ir catalyst on carbon support in MLEFC. The performance of the Pd–Ir–Ni/C catalyst was compared with that of the Pd–Ir/C and Pd–Ni/C catalysts obtained by simultaneous reduction process.

Experimental

Material

The metal precursors used for the preparation of electrocatalysts were $PdCl_2$ (from Aldrich), H_2IrCl_6 (from Alfa Aesar), and $NiCl_2.6H_2O$ (from Aldrich). Vulcan Carbon® XC-72 (particle size 20–40 nm, from E-TEK) was used as a support for the catalysts. Graphite plates (3 cm long and 0.1 cm wide, from E-TEK) were used as substrates for the catalyst to prepare the electrodes. Polytetrafluoroethylene (PTFE) (6% from Aldrich) dispersion was used to make the catalyst slurry. Ethylene glycol (from Merck) was used as the solvent and reduction agent. Ethanol (from Merck), sodium perborate (from Riedel) and H_2SO_4 (from Merck) were used as the fuel, the oxidant and as the electrolyte for electrochemical analysis, respectively. All the chemicals were of analytical grade. Pt/C (40-wt%, from E-TEK) was used as the cathode catalyst.

Catalyst preparation

Carbon supported ternary Pd−Ir−Ni catalysts with different atomic ratios were synthesized by the simultaneous reduction process[17]. Initially, the metal precursors with different atomic ratios were dissolved in deionized water, followed by the addition of carbon support. The resulting mixtures were treated in an ultrasound bath and were refluxed for 3 h under the open atmosphere. After a homogenous suspension is formed 2wt.% $NaBH_4$ and an amount of ammonium citrate (five-fold higher than that the metal (Pd, Ir, and Ni) amount) as a complexing agent and a stabilizer was added to the mixture under steady stirring. Finally, the precipitate was collected by filtration, washed with deionized (DI) water, and dried at 70 ^oC for 2 h. For comparison, the monometallic Pd/C, bimetallic Pd–Ni/C and Pd–Ir/C catalysts were synthesized under the same conditions. The electrocatalytic mixtures and atomic ratios were Pd_{100}/C, $Pd_{40}Ni_{60}/C$, $Pd_{40}Ir_{60}/C$ and $Pd_{35}Ir_5Ni_{60}/C$. The nominal loading of metals in the electrocatalysts was 40 %wt and rest 60 %wt was carbon.

Physical characterization

The morphology of the dispersed catalysts was examined using TEM (Philips CM 12 Transmission Electron Microscope). The particle size distribution and mean particle size were also evaluated using TEM. The crystal structure of the synthesized electrocatalysts was characterized by powder X-ray diffraction (XRD)

using a Rigaku multiflex diffractometer (model RU-200 B) with Cu-$K_{\alpha 1}$ radiation source ($\lambda_{K\alpha 1}$ = 1.5406 A^o) operating at room temperature. The tube current was 40 mA with a tube voltage of 40 kV. The 2θ angular regions between 20º and 90º were recorded at a scan rate of 5° min^{-1}. The mean particle size analyzed from TEM is verified by determining the crystallite size from XRD pattern using Scherer formula.Pt (220) diffraction peak was selected to calculate crystallite size and lattice parameter of platinum. According to Scherrer's equation[18].

$$d = \frac{0.9\lambda_{K\alpha 1}}{ß_{2\theta} \cos \theta_{max}} \qquad (1)$$

where d is the average crystallite size, θ_{max} is the angle at the position of the peak maximum, $ß_{2\theta}$ is the width of the peak (in radians), 0.9 is the shape factor for spherical crystallite and $\lambda_{K\alpha 1}$ is the wavelength of X-rays used. The lattice parameters of the catalysts were estimated according to equation 2 [19]:

$$a = \frac{\sqrt{2}\,\lambda_{K\alpha 1}}{\mathrm{Sin}\,\theta_{max}} \qquad (2)$$

where a, is the lattice parameter (nm) and all the other symbols have the same meanings as in equation 1 [20]. The atomic ratio of the catalysts was determined by an energy dispersive X-ray (EDX) analyzer, which was integrated with the TEM instrument.

Single cell test

In the present study, we fabricated the membraneless ethanol fuel cell (MLEFC) using laminar flow-based fuel cell configuration[21]. In this membraneless fuel cell, ethanol is used as a fuel, sodium perborate is used as an oxidant and sulphuric acid is used as an electrolyte. In crystalline state sodium perborate exist as a dimeric peroxo-salt with water of hydration, but in aqueous solution affords hydrogen peroxide [2] as shown in Eq. (3),

$$[B(OH)_3(O_2H)]^- + H_2O \rightleftharpoons [B(OH)_4]^- + H_2O_2 \qquad (3)$$

In MLEFC, the aqueous fuel and oxidant streams flow in parallel in a single microchannel with the anode and cathode on opposing sidewalls (Fig. 1). Graphite plates of one mm thickness served as current collectors and catalyst support structures. The different anode and cathode catalysts were coated onto the graphite plates. For single cell, the anode catalysts with different atomic ratios were prepared as follows: The catalyst ink was prepared by mixing required quantity of catalyst with a solution of 50 mL of water containing three drops of 6% PTFE dispersion in an ultrasonic bath for 10 min to obtain a uniform dispersion. The catalyst slurry was then spread on the graphite plate by brush and dried at 100 ºC for 30 min to obtain anode and cathode electrodes. The catalysts tested on the anode side were Pd_{100}/C, $Pd_{40}Ni_{60}$/C, $Pd_{40}Ir_{60}$/C and $Pd_{35}Ir_5Ni_{60}$/C with catalyst loading 2 mg/cm^2. On the cathode side, Pd_{100}/C with catalyst loading 2 mg/cm^2 was used in all experiments. The two catalyst-coated graphite plates were aligned to form a channel with 0.1 cm electrode-to-electrode distance (width), a 3 cm length, and a 0.1 cm height. The anolyte (fuel and electrolyte) and catholyte (oxidant and electrolyte) streams flow in a laminar fashion over the anode and cathode, respectively. The electrode area along a microchannel wall between the inlets and the outlet (3 cm long and 0.1 cm wide) was used as the geometric surface area of the electrodes in this study (0.3 cm^2). The design is described in detail elsewhere [1, 22]. The anolyte used in the anode side was 1.0 M ethanol + 0.5 M KOH and the catholyte used in the cathode side was 0.1 M perborate + 1 M KOH. The flow rate of each of the streams was 0.3 mL min^{-1} (total flow rate of 0.6 mL min^{-1}). The MLEFC was operated at room temperature. The current-voltage characteristics of MLEFC were measured using an electrochemical workstation (CH Instruments, model CHI6650, USA) and the data was verified using a multi-meter (MASTECH® MAS830L).

Results and discussions

Physical characterization

X-ray diffraction (XRD)

The XRD patterns of the prepared $Pd_{40}Ni_{60}/C$, $Pd_{40}Ir_{60}/C$ and $Pd_{35}Ir_5Ni_{60}/C$, catalysts are shown in Fig. 1. The peak at 25 – 30° observed in all diffraction patterns of the carbon supported catalysts is attributed to the (0 0 2) plane of hexagonal structure of Vulcan XC-72 carbon support. The diffraction peaks at around 40°, 47°, 68° and 82° are attributed to Pd (111), (200), (220) and (311) crystalline plane respectively, which represents the typical character of crystalline Pd with face centered cubic (FCC) crystalline structure. In case of $Pd_{40}Ir_{60}/C$ and $Pd_{35}Ir_5Ni_{60}/C$, the addition of Ir and Ni atoms to Pd promotes shifts in the Pd-peaks to slightly higher 2θ values, indicating formation of an alloy upon incorporation of Ir and Ni atoms into the palladium fcc structure. No diffraction peaks indicating the presence of pure Ir and Ni or its oxides appeared in the XRD patterns[23,24].

Table 1: The lattice parameters, particle size and the specific area obtained for different atomic ratios of electrocatalysts.

Electrocatalysts	(2 2 0) Diffraction peak position (2θ°)	Lattice parameter (Å)	Average crystallite size from XRD (nm)	Average Particle size from TEM (nm)
Pd_{100}/C	67.54	3.919	2.9	-
$Pd_{40}Ni_{60}/C$	67.89	3.901	3.7	3.4
$Pd_{40}Ir_{60}/C$	67.96	3.898	3.5	3.2
$Pd_{35}Ir_5Ni_{60}/C$	68.02	3.896	4.0	3.6

The lattice parameters and average crystallite size of catalysts obtained from XRD patterns are listed in Table 1. As can be seen from the results in Table 1, the lattice parameter for the $Pd_{40}Ir_{60}/C$ and $Pd_{35}Ir_5Ni_{60}/C$ catalyst are smaller than that of Pd_{100}/C. The decrease in the lattice parameters of the alloy catalysts reflects the progressive increase in the incorporation of Ir and Ni into the alloyed state. The average crystallite sizes calculated by Scherrer formula at peak position Pt (2 2 0) are around 3.7 nm, 3.4 nm and 2.8 nm for $Pd_{40}Ni_{60}/C$, $Pd_{40}Ir_{60}/C$ and $Pd_{35}Ir_5Ni_{60}/C$, respectively.

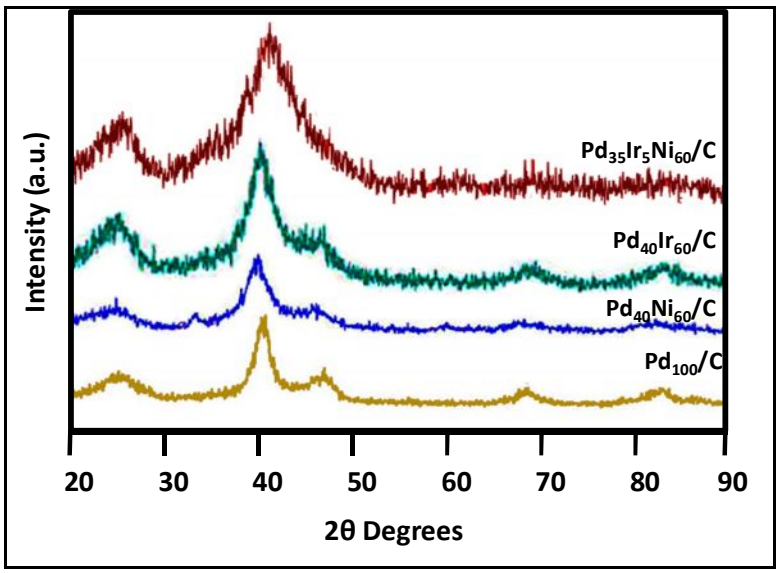

Scanning electron microscopy (SEM)

SEM images of $Pd_{40}Ni_{60}/C$, $Pd_{40}Ir_{60}/C$ and $Pd_{35}Ir_5Ni_{60}/C$ catalysts clearly shows that the nanoparticles of the catalysts are uniformly dispersed on the carbon support and confirms the porous structure of the catalysts prepared.

Transmission electron microscopy (TEM)

The TEM images of the $Pd_{40}Ni_{60}/C$, $Pd_{40}Ir_{60}/C$ and $Pd_{35}Ir_5Ni_{60}/C$ catalysts are presented in Fig. 2a–c, respectively. The metal particles on all the catalysts are spherical in shape and are highly dispersed on the carbon powder support without severe aggregation. The heavy black dots on the carbon support are the catalyst particles. The average size of the metal particles on the prepared catalysts was evaluated from an ensemble of 200 particles in an arbitrarily chosen area of the corresponding TEM images. In comparison to $Pd_{40}Ir_{60}/C$ the mean particle size of $Pd_{35}Ir_5Ni_{60}/C$ were smaller. The particle size distribution of these catalysts is shown in Table 1 in accordance to the TEM images. The mean particle size found by TEM image and XRD analysis were similar.

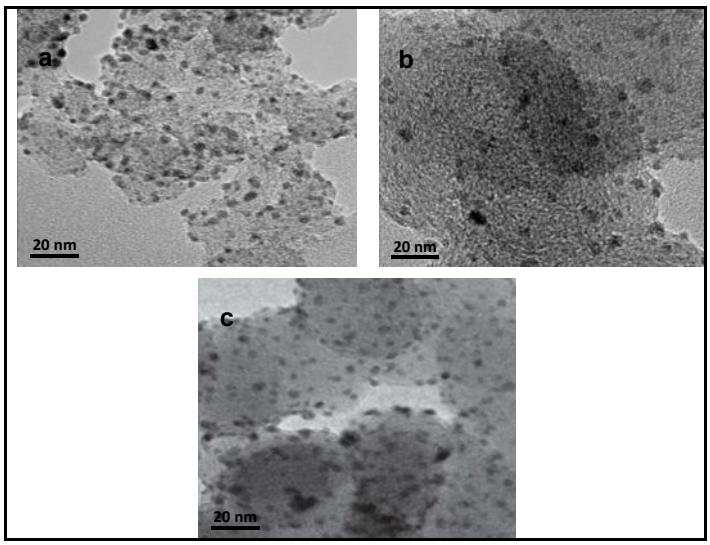

Fig. 2 TEM images of a) $Pd_{40}Ni_{60}/C$, b) $Pd_{40}Ir_{60}/C$ and c) $Pd_{35}Ir_5Ni_{60}/C$ catalysts.

EDX analysis

The EDX analyses of all the $Pd_{40}Ni_{60}/C$, $Pd_{40}Ir_{60}/C$ and $Pd_{35}Ir_5Ni_{60}/C$ catalysts indicates the presence of Pd, Ir and carbon; Pd, Ni and carbon; and both the combinations of Pd, Ir, Ni, and carbon, respectively. The catalysts prepared had the desired elements with some variation in composition. The EDX results of the binary Pd─Ni/C and Pd─Ir/C and the ternary Pd–Ir–Ni/C catalysts are very close to the nominal values, which indicate that the metals were loaded onto the carbon support without obvious loss.

Single cell performance

The microfluidic architecture of laminar flow-based membraneless fuel cells overcomes the fuel crossover and water management issues that plague membrane-based fuel cells (i.e., PEMFC, DMFC) and enables independent control of stream characteristics (i.e., flow-rate and composition). Here we focused on maximizing cell performance, in terms of power density and fuel utilization, by tailoring various structural characteristics and catalytic activity of carbon supported ternary Pd−Ir−Ni catalysts.

The Pd_{100}/C, $Pd_{40}Ni_{60}/C$, $Pd_{40}Ir_{60}/C$ and $Pd_{35}Ir_5Ni_{60}/C$ catalysts were evaluated as anode catalysts for ethanol electro-oxidation by single membraneless ethanol fuel cell (MLEFC), and the data are presented in Fig. 3. The maximum output power density for Pd_{100}/C is 4.36 mW/cm^2. The results of MLEFC adopting to different catalysts are summarized in Table 2. When the current was normalized to the geometric area of single cell, it was observed that the cell performance of $Pd_{35}Ir_5Ni_{60}/C$ catalyst was better than other catalysts. In the low current discharging region, the power drawn from single cell was almost the same for all catalysts except Pd_{100}/C and $Pd_{40}Ni_{60}/C$. However, as the voltage reach around 0.3 V $Pd_{35}Ir_5Ni_{60}/C$ started drawing more current in comparison to others. The open-circuit potential for $Pt_{60}Ru_{40}/C$ catalyst was 0.58 V lower than for $Pd_{35}Ir_5Ni_{60}/C$ (0.73 V). In addition, there was a rapid initial fall in cell voltage for all catalysts, which was due to the slow initial ethanol electro-oxidation reaction at the electrode surface. After an initial drop of 50 mV the change in slope of the polarization curve for $Pd_{35}Ir_5Ni_{60}/C$ decreased, and it started drawing more current. This is attributed to the more effective catalytic ability of $Pd_{35}Ir_5Ni_{60}/C$, once the ethanol electro-oxidation reaction being initiated. Based on peak power density drawn from single cell, $Pd_{35}Ir_5Ni_{60}/C$ is the best anode catalyst with peak power density value of 34.5 mW/cm^2.

Table 2 Summary of performance of single fuel cell tests using (2 mg cm^{-2} catalyst loading, 40 wt% catalyst on carbon)

Anode Catalysts	Open circuit voltage (mV)	Maximum power density (mW/cm^2)	Current density at maximum power density (mA/cm^2)
Pd_{100}/C	0.5	4.36	32.38
$Pd_{40}Ni_{60}/C$	0.51	8.82	68.62
$Pd_{40}Ir_{60}/C$	0.58	19.67	96.95
$Pd_{35}Ir_5Ni_{60}/C$	0.73	34.51	221.63

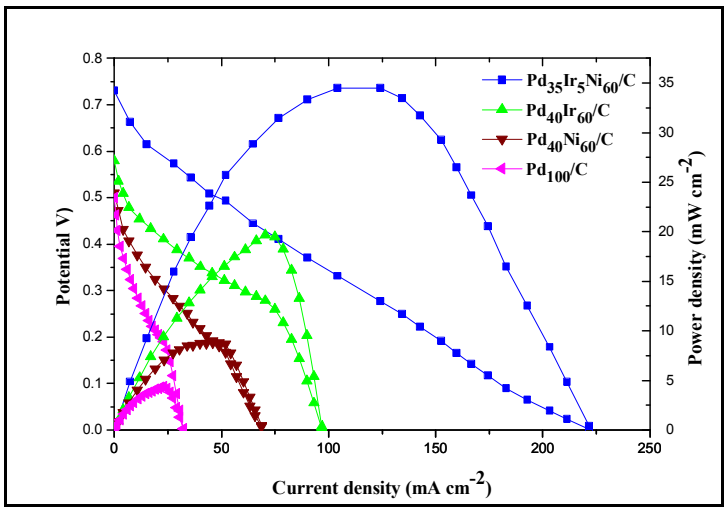

Fig. 3 Polarization and power density curves of different catalyst at 2 mg cm^{-2} catalyst loading on anode and cathode at room temperature.

The addition of Ni is conducive to breaking of C—C bonds in Pd−Ir−Ni/C (35:5:60) blocks the further oxidation of intermediates. This may be due to adsorption of the intermediates on the active sites of the catalysts. In the tri-metallic combinations of Pd, Ir, and Ni, the addition Ir increases the cell performances.

Conclusion

In this work, we observed that the alcohol-reduction process could be effectively used for the preparation of Pd-Ir/C, Pd−Ni/C and Pd−Ir−Ni/C eletrocatalysts for ethanol oxidation. The diffraction peaks at around 40°, 47°, 68° and 82° are attributed to Pd (111), (200), (220) and (311) crystalline plane respectively, which represents the typical character of crystalline Pd with face centered cubic (FCC) crystalline structure. The Pd metal was the predominant material in all the samples, with peaks attributed to the face-centered cubic (fcc) crystalline structure. The SEM and TEM analysis indicated that the catalysts on Vulcan XC-72 carbon support are uniformly dispersed having size of 2 – 4 nm. Additionally, the SEM images confirm the porous structure of the catalysts prepared. EDX analysis indicated that the experimental composition is in agreement with the nominal composition of the catalyst, which confirm the formation Pd−Ir−Ni/C, Pd−Ni/C and Pt−Ir/C metal catalysts having typical Pd crystalline structure and the formation of Pd−Ir alloy. In this work, for the first-time carbon-supported binary Pd−Ni/C, Pd−Ir/C and ternary Pd−Ir−Ni/C anode catalysts were successfully tested in a single membraneless fuel cell using 1.0 M ethanol as the fuel and 0.1 M sodium perborate as the oxidant in the presence of 0.5 M H_2SO_4 as the electrolyte. Based on peak power density drawn from a single cell, Pd−Ir−Ni/C (70:10:20) is the best anode catalyst with peak power density value of 34.5 mW/cm^2 among the catalysts tested. Further work is necessary to characterize the catalysts using different surface analysis techniques and to conduct tests o these electro catalysts in micro fluidic membraneless fuel cells.

References

1. Choban ER, Markoski LJ, Wieckowski A, Kenis PJA., Microfluidic fuel cell based on laminar flow. J Power Sources., 2004,128:54-60.

2. Cohen JL, Westly DA, Pechenik A, Abruna HD., Fabrication and preliminary testing of a planar membraneless microchannel fuel cell, J Power Sources. 2005, 139:96-105.
3. Bazylak A, Sinton D, Djilali N. Improved fuel utilization in microfluidic fuel cells: a computational study. J Power Sources., 2005. 143:57–66.
4. Kjeang E, Djilali N, Sinton D., Microfluidics fuel cells: A review. J Power Sources., 2009, 186:353–369.
5. Carrette L, Friedrich KA, Stimming U., Fuel cells: principles, types, fuels andapplications. Chem Phys Chem., 2000, 1:162–193.
6. Eikerling M, Kornyshev AA, Kuznetsov AM, Ulstrup J, Walbran S., Mechanisms of proton conductance in polymer electrolyte membranes. J Phys Chem B., 2001,105:3646–3662.
7. Priya M, Arun A, Elumalai M, Kiruthika S, Muthukumaran B., A development of Ethanol/Percarbonate membraneless fuel cell. Adv physical chemistry., 2013, 862691:8.
8. Shaegh SAM, Nguyen NT, Chan SH., A membraneless hydrogen peroxide fuel cell using prussian blue as cathode material, Int J Hydrogen Energy., 2011,36:5675-5694.
9. Ponmani K, Durga S, Gowdhamamoorthi M, Kiruthika S, Muthukumaran B. Influence of fuel and media on membraneless sodium percarbonate fuel cell. Ionics., 2014,20:1579-1589.
10. Cotton FA, Wilkinson G (1988) Advanced inorganic chemistry. Wiley Interscience,New York, p 812.
11. Colmati F, Antolini E, Gonzalez ER., Ethanol oxidation on a carbon-supported $Pt_{75}Sn_{25}$ electrocatalyst prepared by reduction with formic acid: Effect of thermal treatment. Appl Catal B., 2007, 73:106-115.
12. Radmilovic V, Gasteiger HA , Ross Jr. PN (1995) Structure and Chemical Composition of a Supported Pt-Ru Electrocatalyst for Methanol Oxidation, J. Catal., 154:98–106.
13. Beyhan S, Leger J-M, Kadırgan F., Pronounced synergetic effect of the nano-sized PtSnNi/C catalyst for ethanol oxidation in direct ethanol fuel cell Applied Catalysis B: Environmental., 2013, 130–131:305–313.
14. Arun A, Gowdhamamoorthi M, Kiruthika S, Muthukumaran B., Analysis of membraneless methanol fuel cell using percarbonate as an oxidant, J of The Electrochemical Society., 2013, 161:F1-F7.
15. Ponmani K, Durga S, Gowdhamamoorthi M, Kiruthika S, Muthukumaran B., Influence of fuel and media on membraneless sodium percarbonate fuel cell, Ionics, 2014, 20:1579-1589.
16. Cotton FA, Wilkinson G., Advanced inorganic chemistry. Wiley Interscience,New York, 1988, 812.
17. Jayashree RS, Yoon SK, Brushett FR, Lopez-Montesinos PO, Natarajan D, Markoski LJ, Kenis PJA., On the performance of membraneless laminar flow-based fuel cells, Journal of Power Sources., 2010,195:3569–3578.
18. He Q, Chen W, Chen S, Laufek F, Mukerjee S., Carbon Supported PdM (M=Au and Sn) nanocatalysts for the Electro-oxidation of Ethanol in High pH Media, J Power Sources., 2009, 187:298-304.
19. Qiu CC, Shang R, Xie YF, Bu YR, Li CY, Ma HY., Electrocatalytic activity of bimetallic Pd-Ni thin films towards the oxidation of methanol and ethanol. Mater Chem Phys., 2010,120:323-330.
20. Bagchi J, Bhattacharya SK., Electrocatalytic activity of binary palladium ruthenium anode catalyst on Ni-support for ethanol alkaline fuel cells, Trans Metal Chemistry.,2007, 32(1):47-55.
21. Ksar F, Ramos L, Keita B, Nadjo L, Beaunier P, Remita H., Bimetalic palladium-gold nanostructures application in ethanol oxidation. Chem Mater., 2009,21:3677-3683.
22. Jou LS, Chang JK, Twhang TJ, Sun IW., Electrodeposition of palladium-copper films from 1-ethyl-3-methylimidazolium chloride-tetrafluoroborate ionic liquid on indium tin oxide electrode, J Electrochem Soc., 2009,156(6):193-197.
23. Shen SY, Zhao TS, Xu JB, Li YS., Synthesis of PdNi Catalysts for the oxidation of ethanol in alkaline direct ethanol fuel cells, J. Power Sources., 2010, 195:1001-1006.
24. Shen SY, Zhao TS, Jianbo X, Yinshi L., High performance of a carbon supported ternary PdIrNi catalyst for ethanol electro-oxidation in anion-exchange membrane direct ethanol fuel cells, Energy & Environmental Science, 2011, 4:1428-1433.

*****